

Optimal Transport Event Representation for Anomaly Detection

Aditya Bhargava,¹ Tianji Cai,^{2,3,*} and Benjamin Nachman^{4,5}

¹*Department of Physics, University of California, Berkeley, CA 94720, USA*

²*School of Physical Science and Engineering, Tongji University, Shanghai 200092, China*

³*State Key Laboratory of Autonomous Intelligent Unmanned Systems,*

MOE Frontiers Science Center for Intelligent Autonomous Systems, Tongji University, Shanghai 200092, China

⁴*Department of Particle Physics and Astrophysics, Stanford University, Stanford, CA 94305, USA*

⁵*Fundamental Physics Directorate, SLAC National Accelerator Laboratory, Menlo Park, CA 94025, USA*
(Dated: December 5, 2025)

We introduce optimal transport (OT) as a physics-based intermediate event representation for weakly supervised anomaly detection. With only 0.5% injection of resonant signals in the LHC Olympics benchmark datasets, the OT-augmented feature set achieves nearly twice the significance improvement of standard high-level observables, while end-to-end deep learning on low-level four-momenta struggles in the low-signal regime. The gains persist across signal types and classifiers, underscoring the value of structured representations in machine learning for anomaly detection.

Introduction — As targeted searches struggle to find new physics beyond the Standard Model, alternative model-agnostic strategies have become increasingly important. Anomaly detection (AD), powered by modern machine learning (ML), offers a promising route to identify rare or unexpected signals without specific model hypotheses [1–4]. A prominent class of AD frameworks follows the *weak supervision* (WS) paradigm [5–8], where classifiers are trained to distinguish between signal-rich data and background-only references. These approaches are particularly effective for resonant anomalies, i.e., localized signals atop smooth background distributions, and have been successfully deployed to experimental data [9–14].

Methods within the WS paradigm differ primarily in background modeling and classifier design [15–20], both of which depend on the underlying event representation. Most studies use a number of standard high-level observables to summarize the event, which may restrict the scope of detectable signals if the chosen observables cannot capture signal characteristics. To broaden sensitivity, recent works [17, 21] used as inputs a maximal feature set, i.e., the final-state kinematics of an event. While powerful, methods based on low-level four-momenta usually require training (or pre-training [21]) a large (foundation) model on substantial amounts of data, and are typically less effective in the (ultra) low-signal regime where anomaly detection is most needed.

We propose an alternative approach that exploits full final-state kinematics while avoiding sophisticated, resource-intensive models and extensive training data. In particular, *optimal transport* (OT) theory is introduced to define a novel intermediate representation, capturing essential event structures in a compact and structured form. OT defines a distance between probability distributions by computing the most efficient way to transform one into another [22]. Its sensitivity to geometric structure has been utilized to equip the space of collider events with physically meaningful metrics [23–30], show-

ing promises across collider applications including jet and event classification [31, 32], calibration [33], and more recently, anomaly detection at the event level [34–36].

Nonetheless, the full potential of optimal transport as a *standalone event representation* remains largely untapped. Here we propose the key conceptual shift: rather than merely using OT to define metrics between events, we develop an efficient representation through its linearization. When combined with standard high-level observables, features derived from this OT representation yield significant improvements for resonant anomaly detection, particularly in the low-signal regime. Remarkably, only a small number of OT-based features are needed to boost performance. These results highlight the value of physically grounded representations as a bridge between engineered features and fully end-to-end machine learning, encouraging further exploration of model latent spaces and alternative intermediate representations.

Datasets and Weak Supervision Framework — We use datasets from the 2020 LHC Olympics (LHCO) Anomaly Detection Challenge [1, 37, 38], which includes two signal-injected sets (R&D1 and R&D2) and a background-only set. Each R&D dataset contains one million QCD dijet events and 100 thousand signal events from a resonant decay $W' \rightarrow XY$ with $m_{W'}, m_X, m_Y = 3.5 \text{ TeV}, 500 \text{ GeV}, 100 \text{ GeV}$, respectively. In R&D1, $X, Y \rightarrow qq$, producing two-pronged jets; in R&D2, $X, Y \rightarrow qqq$, yielding three-prong substructure.

Events are simulated in `Pythia 8` [39, 40] and `Delphes 3.4.1` [41–43], whereas jets are clustered in `Fastjet` [44] via the anti- k_T algorithm with $R = 1$. Events whose leading jet has $p_T > 1.2 \text{ TeV}$ are selected. Only particles in the two leading- p_T jets are retained, which are expected to contain the X/Y decay products. The signal region (SR) is defined as $m_{JJ} \in [3.3, 3.7] \text{ TeV}$, with its complement forming the sideband regions (SB). This is chosen for consistency with prior works [15, 17]. Each

R&D dataset is further augmented with $\sim 610\text{k}$ background events in the SR from Ref. [38], yielding $\sim 731\text{k}$ background and $\sim 75\text{k}$ signal events in total.

Weak supervision trains on mixed samples without requiring event-level labels or class proportions, and is provably as powerful as full supervision by the Neyman–Pearson lemma in asymptotic limit [45]. This underlies the *classification without labels* (CWoLa) framework [6], where recent CWoLa-based anomaly detectors model SR background by interpolating SB data via classifiers [46], density estimation [18, 19], generative models [15], and invertible networks [47]. These methods are now capable of near optimal matching. We therefore assume perfect background interpolation and adopt an *idealized anomaly detector* (IAD) [15], which enables us to isolate the effect of our new representation and to establish an upper bound on its performance within the WS framework.

Two training sets (A1 and A2) are constructed in the signal region. The set A1 contains only background events (labeled 0), whereas the set A2 includes background plus a fixed fraction of signal events, i.e., S/B=0.5%, 0.63%, 0.7%, 0.8%, 1%, 1.2%, 1.4%, 1.6%, 10%, covering a large spectrum of possible signal amounts. In total, there are nine A2 sets, one for each S/B level, and all events in A2 are labeled 1. Classifiers are then trained to distinguish events in A1 from those in A2, using only dataset-level labels. The main results use boosted decision trees (BDTs) [48, 49] as the classifier, thanks to its robustness to noises and correlated features. Results using multilayer perceptrons (MLPs) are presented in the Appendix. To reduce statistical fluctuations, we aggregate over 50 independently trained BDT classifiers (10 for MLPs as in [15]) to obtain the results for one ensemble, and further average over 10 ensembles to estimate the mean and the spread.¹ Performance is evaluated using event-level labels on two separate test sets—background-only B1 and signal-only B2. On the statistical level, our datasets match those used in Ref. [15], with A1 having 272k background events, A2 containing 121,352 background events plus injected signal events, B1 having 340k background events, and B2 having 20k signal events—all within the SR.

Optimal Transport Representation and Features — Standard analyses rely on high-level observables such as jet mass and n -subjettiness ratios. The LHC R&D1 itself provides $\{m_{J_1}, m_{J_2}, \tau_{21}^{J_1}, \tau_{21}^{J_2}\}$ for the two leading jets, whereas R&D2 adds $\{\tau_{32}^{J_1}, \tau_{32}^{J_2}\}$. In contrast, we propose an intermediate representation based on particle four-momenta, using a specific OT distance called

the 2-Wasserstein metric (W_2). For a pair of events \mathcal{E} and $\tilde{\mathcal{E}}$ containing massless constituent particles at $x_i, \tilde{x}_j \in (y, \phi) \subseteq \mathbb{R}^2$ with normalized transverse momenta p_T^i, \tilde{p}_T^j respectively, the 2-Wasserstein distance is defined as

$$W_2(\mathcal{E}, \tilde{\mathcal{E}}) = \min_{g_{ij} \in \Gamma(\mathcal{E}, \tilde{\mathcal{E}})} \left(\sum_{ij} g_{ij} \|x_i - \tilde{x}_j\|^2 \right)^{1/2}, \quad (1)$$

$$\Gamma(\mathcal{E}, \tilde{\mathcal{E}}) = \left\{ g_{ij} : g_{ij} \geq 0, \sum_j g_{ij} = p_T^i, \sum_i g_{ij} = \tilde{p}_T^j \right\},$$

where $\Gamma(\mathcal{E}, \tilde{\mathcal{E}})$ contains the transport plans that move g_{ij} amount of p_T from particle i in \mathcal{E} to particle j in $\tilde{\mathcal{E}}$ over a distance $\|x_i - \tilde{x}_j\|$ on the y – ϕ plane. Thus, W_2 quantifies the minimal *cost* to morph one event into another and is by definition infrared and collinear (IRC) safe.

To convert the pairwise distance into an event representation, we employ the linearization method originally introduced to reduce OT’s computational cost [25, 50]. The linearized W_2 (Lin W_2) embeds each event into the tangent space at a fixed reference event \mathcal{R} containing particles with $p_T = R_i$ at $y_i \in (y, \phi)$. Its i -th component is given by

$$\text{Lin}W_2^i(\mathcal{E})|_{\mathcal{R}} := \frac{1}{\sqrt{R_i}} \sum_j r_{ij} x_j \quad \text{for } i \in [1, R], \quad (2)$$

where r_{ij} is an optimal transport plan from \mathcal{R} to \mathcal{E} and the RHS gives the p_T -weighted barycenter of where each reference particle is mapped. Since $x_j = (y_j, \phi_j)$, $\text{Lin}W_2^i$ is itself a vector in \mathbb{R}^2 , resulting in a $2R$ -dimensional embedding for each event which is likewise IRC-safe. Instead of treating Lin W_2 as merely an efficient approximation to the original W_2 distance, here we highlight this novel representation in its own right, marking a major conceptual shift.

In practice, the Lin W_2 embedding is applied at the jet level, where each jet is preprocessed by centering its axis and vertically aligning the principal component of its transverse momentum flow. The reference jet \mathcal{R} is constructed as a 10×10 grid over the (y, ϕ) plane, with every particle assigned a uniform $p_T = \frac{1}{100}$.² To obtain the representation for an entire event, we concatenate the Lin W_2 embeddings of the two leading jets, yielding a Euclidean vector in $\mathbb{R}^{2 \times 100 \times 2 = 400}$; extensions to a more

¹ A tree consists of 200 iterations with up to 31 leaf nodes. An MLP has three hidden layers, each with 64 ReLU units. We found the results to be robust to reasonable architectural variations and did not further optimize model hyperparameters.

² The mathematical advantages of using a uniform reference jet were established in [25]. The impact of alternative, including non-uniform, references has been analyzed in [26, 50] and found to be minimal provided the reference is neither too concentrated nor too sparse. Accordingly, we adopt a uniform reference with a number of constituents comparable to that of particles in a typical jet.

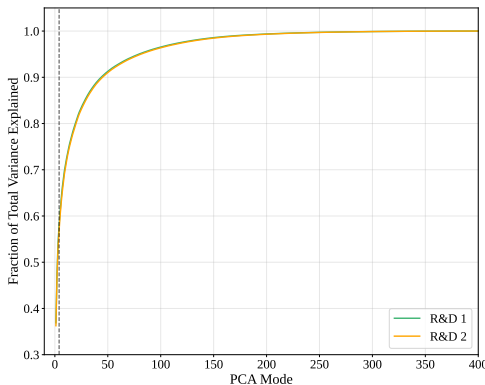


FIG. 1: Total variance explained by increasing numbers of PCA modes of the OT representations for 10k samples from the R&D1 dataset (*green*) and the R&D2 dataset (*orange*).

general multiscale OT treatment for an entire collider event [32] are left to future work. Constructing the OT representation scales at most as $\mathcal{O}(n^3)$ in the number of particles in the reference jet \mathcal{R} , which is negligible for $n \sim \mathcal{O}(100)$ and is further parallelizable across events under the linearization scheme.

From the high-dimensional OT representation, we further extract features using a principal component analysis (PCA). For a sample dataset with 5k background and 5k signal events randomly selected from R&D1 or R&D2, the leading four modes account for almost 60% of the variance, and 100 modes suffice to capture more than 95% of total data variance; see Fig. 1. Accordingly, we construct a new feature set from the first hundred PCA components of the OT representation, which serves as additional high-level inputs for anomaly detection.

Results — Fig. 2 shows the maximum significance improvement (SI) obtained by scanning the signal-to-background ratio (S/B) from 0.2% to 10% for the R&D1 and R&D2 datasets using BDT ensembles as the classifier. At low signal injection levels ($S/B \lesssim 1.6\%$), feature sets augmented with the first k PCA modes of the OT representation (OT_k) consistently outperform both standard high-level observables and the low-level full phase space (PS) method of Ref. [17]. In the ultra-low regime ($S/B \lesssim 0.7\%$), OT_k even exceeds the pre-trained foundation model (OmniLearn) of Ref. [21], despite the latter’s substantially greater computational cost. Fig. 3 in the Appendix further displays the full SI curves at a representative $S/B = 0.63\%$.

On R&D1, the enhancement is most pronounced in the ultra-low to low signal regime, where approaches based on the full phase space and foundation models both suffer from limited signal statistics, with the latter alleviating the issue to some extent through large-scale pretraining. With less than 0.5% signal injection, OT-augmented fea-

ture sets raise the maximum SI to $\gtrsim 25$, more than an order of magnitude above the low-level baselines and $\sim 65\%$ above the standard high-level observable set. The performance of OT_k (except $k = 100$) remains stable across the entire range of signal fractions. Similar gains are observed in the less-studied R&D2 dataset, albeit with a smaller margin over the standard observables. No full phase space or foundation model benchmark currently exists for R&D2; based on the R&D1 comparison, comparable trends are likely and we encourage future studies to strengthen the low-level benchmarks.

Only a few OT features are needed to achieve the observed gains. The first 3–5 PCA components already saturate the maximum SI, with negligible benefit beyond $k \approx 6$, consistent with the variance profile in Fig. 1. Using very large OT feature sets (e.g., OT_{100}) degrades performance for $S/B \lesssim 0.6\%$, partially reflecting the difficulty of training BDT ensembles with many correlated inputs. The effect is even stronger for MLP classifiers; see Fig. 4 in the Appendix. This illustrates a fundamental trade-off in anomaly detection: expanding the feature set increases the information accessible to more expressive classifiers, but also requires higher signal statistics for effective training. Consequently, well-designed representations and careful feature selection are essential for maximizing discriminative power and attaining optimal sensitivity, especially in the low-signal regime.

In the high-signal regime ($\sim 10\%$), the two low-level approaches perform best, reaching a maximum SI of 50 on R&D1, consistent with their ability to exploit raw four-momenta when ample signal is present. OT_{100} attains a max SI of 33, $\sim 20\%$ above OT_{3-6} and nearly 80% above the standard observable set $\{m_{J_1}, m_{J_2}, \tau_{21}^{J_1}, \tau_{21}^{J_2}\}$. An analogous pattern appears in R&D2 at $S/B=10\%$, where OT_{100} reaches a max SI ≈ 32 , more than doubling the performance of the corresponding jet mass and n -subjettiness ratio inputs. The gap between OT_{100} and the low-level methods may be due to information encoded in IRC-unsafe aspects of the event. Since the OT representation is IRC-safe by construction, its gains are expected to be more robust across signal types and more transferable from simulations to data.

An ablation study on R&D1 at $S/B=0.63\%$ further isolates the role of OT features; see Fig. 5 in the Appendix. OT features alone, without m_J or τ_{21} , do not yield competitive performance. However, including jet masses and at least the first four OT modes raises the maximum SI to ~ 18 , matching the performance of the standard observable set in Fig. 2. This confirms that OT features encodes similar prong-sensitive morphological information as n -subjettiness, while the absence of explicit jet-mass information in the current OT construction explains the lower SI (~ 12) obtained when the inputs include only τ_{21} and OT_{3-6} .

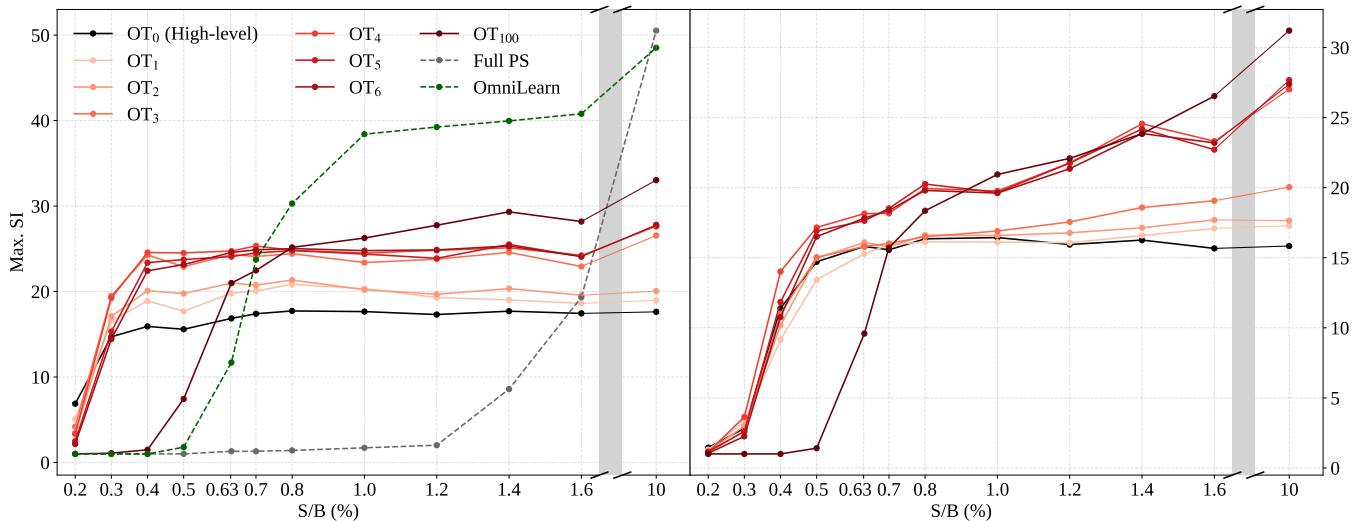


FIG. 2: Maximum Significance Improvement (SI) for the R&D1 (*left*) and R&D2 (*right*) datasets using BDT ensembles as the classifier, with the signal injection level S/B varying from 0.2% to 10%. The group of red curves represent increasing numbers of OT features added to standard high-level observables, i.e., $\{m_{J_1}, m_{J_2}, \tau_{21}^{J_1}, \tau_{21}^{J_2}\}$ for R&D1, and $\{m_{J_1}, m_{J_2}, \tau_{21}^{J_1}, \tau_{21}^{J_2}, \tau_{32}^{J_1}, \tau_{32}^{J_2}\}$ for R&D2. The dashed gray line in the left subplot shows the max SI values from Ref. [17] using full phase space as inputs to dedicated models, whereas the dashed green line shows the performance of the pre-trained foundation model OmniLearn from Ref. [21].

Conclusions — We presented a physics-aware, intermediate representation of collider events based on optimal transport, enabling highly effective resonant anomaly detection. Notably, enhancing standard high-level observables with only a couple of features derived from the OT representation leads to a significance improvement of more than 25 at a signal injection level of only $\sim 0.5\%$ for the LHC R&D1 dataset, with comparable performance gain also observed on R&D2. Our method outperforms both ends of the spectrum—standard high-level observables and end-to-end machine learning (foundation models included) on low-level particle four-momenta.

Several extensions could further enhance performance. While principal component analysis was employed for its simplicity and efficiency, more expressive approaches to feature extraction could be explored. Likewise, advanced classifiers such as neural networks may enable direct use of the OT representation without dimensionality reduction. Conversely, the surprising effectiveness of the simple PCA method underscores the importance of carefully balancing data and computational efficiency when introducing sophisticated models, particularly in the low-signal regime.

Beyond boosted dijet signals, our framework can be applied to more complex event topologies. OT-based observables have shown success in characterizing high-multiplicity, quasi-isotropic radiation patterns typical of hidden-valley scenarios [51]. For events featuring distinct total transverse momenta and multiple intrinsic scales,

more flexible OT representations with additional degrees of freedom may be required [32, 50]. The framework can also be generalized to incorporate information beyond event kinematics, such as particle ID, through multi-species vector-valued optimal transport [52]. Furthermore, preliminary results indicate that our method may be applicable to non-resonant anomaly detection, which may open a largely unexplored landscape for new physics discovery.

The code for the analysis can be found at <https://github.com/TianjiCai/ADwithOT>.

Acknowledgments — The authors would like to thank Michael Krämer and Vinicius Mikuni for useful discussions. The work of TC is supported by the Fundamental Research Funds for the Central Universities. BN is supported by the U.S. Department of Energy (DOE), Office of Science under contract DE-AC02-76SF00515. This research used resources of the National Energy Research Scientific Computing Center, a DOE Office of Science User Facility supported by the Office of Science of the U.S. Department of Energy under Contract No. DE-AC02-05CH11231.

* Contact author: tianji-cai@tongji.edu.cn

[1] G. Kasieczka and *et al.*, The lhc olympics 2020 a community challenge for anomaly detection in high energy physics, Reports on Progress in Physics **84**, 124201 (2021), arXiv:2101.08320.

- [2] T. Aarrestad *et al.*, The Dark Machines Anomaly Score Challenge: Benchmark Data and Model Independent Event Classification for the Large Hadron Collider, *SciPost Phys.* **12**, 043 (2022), arXiv:2105.14027 [hep-ph].
- [3] G. Karagiorgi, G. Kasieczka, S. Kravitz, B. Nachman, and D. Shih, Machine learning in the search for new fundamental physics (2021), arXiv:2112.03769 [hep-ph].
- [4] V. Belis, P. Odagiu, and T. K. Aarrestad, Machine learning for anomaly detection in particle physics, *Reviews in Physics* **12**, 100091 (2024).
- [5] J. Hernández-González, I. Inza, and J. A. Lozano, Weak supervision and other non-standard classification problems: A taxonomy, *Pattern Recognition Letters* **69**, 49 (2016).
- [6] E. M. Metodiev, B. Nachman, and J. Thaler, Classification without labels: Learning from mixed samples in high energy physics, *JHEP* **10**, 174, arXiv:1708.02949 [hep-ph].
- [7] J. Collins, K. Howe, and B. Nachman, Anomaly detection for resonant new physics with machine learning, *Phys. Rev. Lett.* **121**, 241803 (2018).
- [8] R. T. D’Agnolo and A. Wulzer, Learning new physics from a machine, *Physical Review D* **99**, 10.1103/physrevd.99.015014 (2019).
- [9] G. e. a. Aad (ATLAS Collaboration), Weakly supervised anomaly detection for resonant new physics in the dijet final state using proton-proton collisions at $\sqrt{s} = 13$ TeV with the atlas detector, *Phys. Rev. D* **112**, 072009 (2025).
- [10] R. Gambhir, R. Mastandrea, B. Nachman, and J. Thaler, Isolating unisolated upsilons with anomaly detection in cms open data, *Phys. Rev. Lett.* **135**, 021902 (2025).
- [11] T. A. Vami and D. Zhang, Search for black holes and sphalerons using novel machine learning techniques at cms (2025), arXiv:2511.10662 [hep-ex].
- [12] D. Shih, M. R. Buckley, L. Necib, and J. Tamanas, via machinae: Searching for stellar streams using unsupervised machine learning, *Monthly Notices of the Royal Astronomical Society* **509**, 5992 (2021), <https://academic.oup.com/mnras/article-pdf/509/4/5992/41764058/stab3372.pdf>.
- [13] D. Shih, M. R. Buckley, and L. Necib, Via machinae 2.0: Full-sky, model-agnostic search for stellar streams in gaia dr2, *Monthly Notices of the Royal Astronomical Society* **529**, 4745 (2024), <https://academic.oup.com/mnras/article-pdf/529/4/4745/57162125/stae446.pdf>.
- [14] A. Hallin, D. Shih, C. Krause, and M. R. Buckley, Via Machinae 3.0: A search for stellar streams in Gaia with the CATHODE algorithm, (2025), arXiv:2509.08064 [astro-ph.GA].
- [15] A. Hallin, J. Isaacson, G. Kasieczka, C. Krause, B. Nachman, T. Quadfasel, M. Schlaffer, D. Shih, and M. Sommerhalder, Classifying anomalies through outer density estimation, *Physical Review D* **106**, 10.1103/physrevd.106.055006 (2022), arXiv:2109.00546.
- [16] K. Benkendorfer, L. Le Pottier, and B. Nachman, Simulation-assisted decorrelation for resonant anomaly detection, *Phys. Rev. D* **104**, 035003 (2021), arXiv:2009.02205.
- [17] E. Buhmann, C. Ewen, G. Kasieczka, V. Mikuni, B. Nachman, and D. Shih, Full phase space resonant anomaly detection, *Phys. Rev. D* **109**, 055015 (2024), arXiv:2310.06897 [hep-ph].
- [18] B. Nachman and D. Shih, Anomaly detection with density estimation, *Physical Review D* **101**, 10.1103/physrevd.101.075042 (2020).
- [19] G. Stein, U. Seljak, and B. Dai, Unsupervised indistribution anomaly detection of new physics through conditional density estimation (2020), arXiv:2012.11638 [cs.LG].
- [20] C. L. Cheng, G. Singh, and B. Nachman, Incorporating physical priors into weakly supervised anomaly detection, *Phys. Rev. Lett.* **135**, 021801 (2025).
- [21] V. Mikuni and B. Nachman, Method to simultaneously facilitate all jet physics tasks, *Phys. Rev. D* **111**, 054015 (2025), arXiv:2404.16091.
- [22] G. Peyré and M. Cuturi, Computational optimal transport (2020), arXiv:1803.00567 [stat.ML].
- [23] P. T. Komiske, E. M. Metodiev, and J. Thaler, Metric Space of Collider Events, *Phys. Rev. Lett.* **123**, 041801 (2019), arXiv:1902.02346 [hep-ph].
- [24] T. Cai, *Optimal Transport for High Energy Physics*, Ph.D. thesis, UC, Santa Barbara (main) (2023).
- [25] T. Cai, J. Cheng, N. Craig, and K. Craig, Linearized optimal transport for collider events, *Phys. Rev. D* **102**, 116019 (2020).
- [26] T. Cai, J. Cheng, K. Craig, and N. Craig, Which metric on the space of collider events?, *Phys. Rev. D* **105**, 076003 (2022).
- [27] T. Cai, J. Cheng, N. Craig, G. Koszegi, and A. J. Larkoski, The phase space distance between collider events (2024), arXiv:2405.16698 [hep-ph].
- [28] P. T. Komiske, E. M. Metodiev, and J. Thaler, The Hidden Geometry of Particle Collisions, *JHEP* **07**, 006, arXiv:2004.04159 [hep-ph].
- [29] A. J. Larkoski and J. Thaler, A Spectral Metric for Collider Geometry, (2023), arXiv:2305.03751 [hep-ph].
- [30] R. Gambhir, A. J. Larkoski, and J. Thaler, SPECTER: efficient evaluation of the spectral EMD, *JHEP* **12**, 219, arXiv:2410.05379 [hep-ph].
- [31] P. Onyisi, D. Shen, and J. Thaler, Comparing point cloud strategies for collider event classification, *Physical Review D* **108**, 10.1103/physrevd.108.012001 (2023).
- [32] T. Cai, N. Craig, K. Craig, and X. Lin, Multiscale optimal transport for complete collider events, *Phys. Rev. D* **112**, 036021 (2025), arXiv:2501.10681.
- [33] G. e. a. Aad (ATLAS), A continuous calibration of the ATLAS flavour-tagging classifiers via optimal transportation maps, *Eur. Phys. J. C* **85**, 1272 (2025), arXiv:2505.13063 [hep-ex].
- [34] N. Craig, J. N. Howard, and H. Li, Exploring Optimal Transport for Event-Level Anomaly Detection at the Large Hadron Collider, (2024), arXiv:2401.15542 [hep-ph].
- [35] L. Brennan, T. A. Vami, O. Amram, S. Sekhar, Y. Takahashi, L. Moureaux, M. Sommerhalder, P. Maksimovic, T. Cai, and N. Craig, Weakly supervised anomaly detection with event-level variables, *Phys. Rev. D* **112**, 055040 (2025), arXiv:2504.13249.
- [36] R. T. D’Agnolo, A. Glioti, G. Rigo, and A. Valenti, The intrinsic dimension of collider events and model-independent searches in 100 dimensions (2025), arXiv:2511.20760 [hep-ph].
- [37] G. Kasieczka, B. Nachman, and D. Shih, R&D Dataset for LHC Olympics 2020 Anomaly Detection Challenge, 10.5281/zenodo.6466204 (2022).
- [38] D. Shih, Additional QCD Background Events for LHC02020 R&D (signal region only), 10.5281/zen-

- odo.8370758 (2023).
- [39] T. Sjostrand, S. Mrenna, and P. Z. Skands, PYTHIA 6.4 Physics and Manual, JHEP **05**, 026, arXiv:hep-ph/0603175 [hep-ph].
 - [40] T. Sjostrand, S. Mrenna, and P. Z. Skands, A Brief Introduction to PYTHIA 8.1, Comput. Phys. Commun. **178**, 852 (2008), arXiv:0710.3820 [hep-ph].
 - [41] J. de Favereau, C. Delaere, P. Demin, A. Giammanco, V. Lemaitre, A. Mertens, and M. Selvaggi, DELPHES 3: A modular framework for fast simulation of a generic collider experiment, JHEP **02**, 057, arXiv:1307.6346 [hep-ex].
 - [42] M. Selvaggi, DELPHES 3: A modular framework for fast-simulation of generic collider experiments, in *Proceedings, 15th International Workshop on Advanced Computing and Analysis Techniques in Physics Research (ACAT 2013): Beijing, China, May 16-21, 2013*, Vol. 523 (2014) p. 012033.
 - [43] A. Mertens, New features in Delphes 3, in *Proceedings, 16th International Workshop on Advanced Computing and Analysis Techniques in Physics (ACAT 14): Prague, Czech Republic, September 1-5, 2014*, Vol. 608 (2015) p. 012045.
 - [44] M. Cacciari, G. P. Salam, and G. Soyez, Fastjet user manual, The European Physical Journal C **72**, 10.1140/epjc/s10052-012-1896-2 (2012).
 - [45] J. Neyman, E. S. Pearson, and K. Pearson, IX. on the problem of the most efficient tests of statistical hypotheses, Philosophical Transactions of the Royal Society of London. Series A, Containing Papers of a Mathematical or Physical Character **231**, 289 (1933).
 - [46] A. Andreassen, B. Nachman, and D. Shih, Simulation assisted likelihood-free anomaly detection, Phys. Rev. D **101**, 095004 (2020), arXiv:2001.05001.
 - [47] J. A. Raine, S. Klein, D. Sengupta, and T. Golling, CURTAINS for your sliding window: Constructing unobserved regions by transforming adjacent intervals, Front. Big Data **6**, 899345 (2023), arXiv:2203.09470 [hep-ph].
 - [48] T. Finke, M. Hein, G. Kasieczka, M. Krämer, A. Mück, P. Prangchaikul, T. Quadfasel, D. Shih, and M. Sommerhalder, Tree-based algorithms for weakly supervised anomaly detection, Phys. Rev. D **109**, 034033 (2024), arXiv:2309.13111.
 - [49] M. Freytsis, M. Perelstein, and Y. C. San, Anomaly detection in the presence of irrelevant features, Journal of High Energy Physics **2024**, 220 (2024).
 - [50] T. Cai, J. Cheng, B. Schmitzer, and M. Thorpe, The linearized hellinger–kantorovich distance, SIAM Journal on Imaging Sciences **15**, 45 (2022), arXiv:2102.08807.
 - [51] C. Cesarotti and J. Thaler, A robust measure of event isotropy at colliders (2020), arXiv:2004.06125 [hep-ph].
 - [52] K. Craig, N. G. Trillos, and D. Nikolić, Vector valued optimal transport: from dynamic to static formulations (2025), arXiv:2505.03670 [math.AP].

APPENDIX

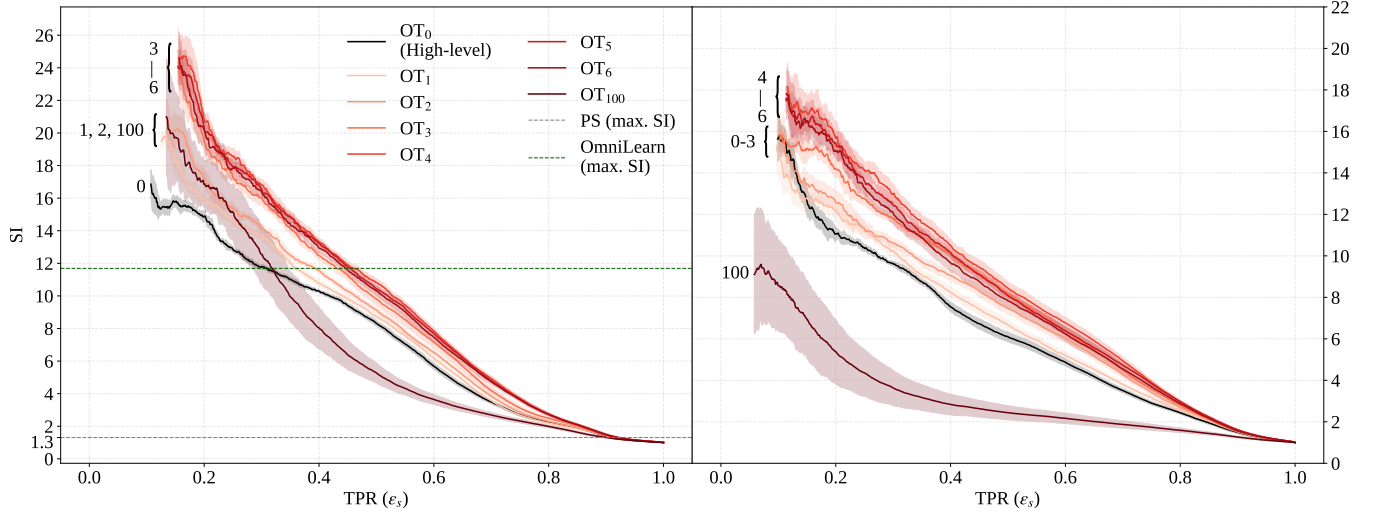


FIG. 3: Significance Improvement (SI) curves for the R&D1 (*left*) and R&D2 (*right*) datasets at a representative signal injection level of $S/B = 0.63\%$, using BDT ensembles as the classifier. The group of red curves represent increasing numbers of OT features added to standard high-level observables, with shaded bands indicating 1σ variations across the BDT ensembles. For R&D1, the dashed gray line shows the maximum SI values of the full phase space method from Ref. [17], and the dashed green line shows that of the pretrained foundation model OmniLearn from Ref. [21].

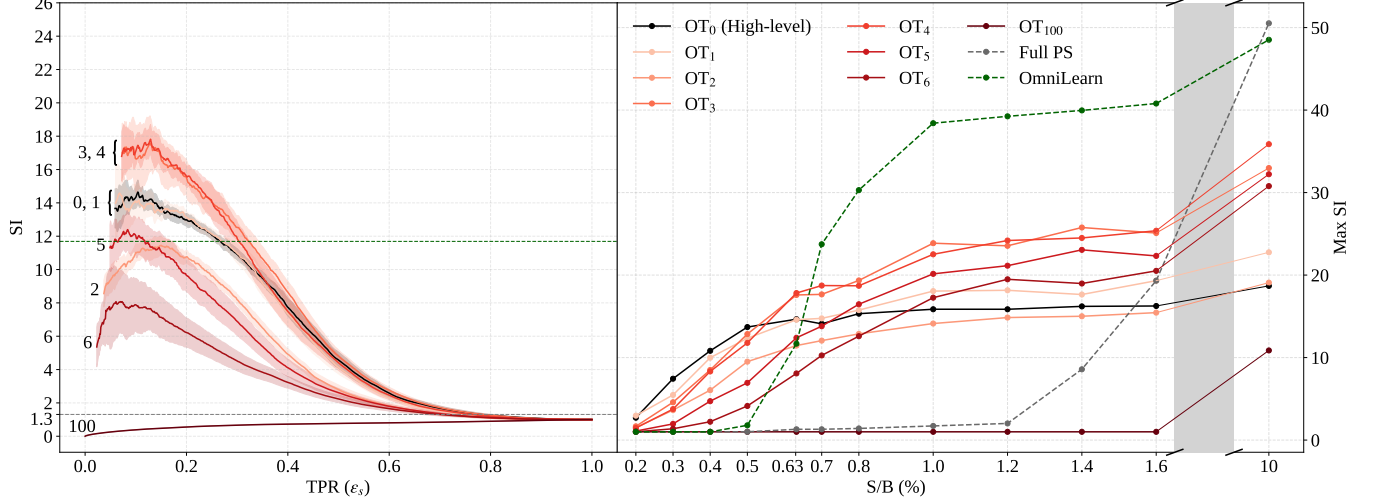


FIG. 4: Anomaly detection for the R&D1 dataset using MLP ensembles as the classifier. *Left*: The SI curves at the signal injection level $S/B = 0.63\%$. *Right*: Maximum SI at S/B between 0.2% and 10% . The group of red curves represent increasing numbers of OT features added to standard high-level observables $\{m_{J_1}, m_{J_2}, \tau_{21}^{J_1}, \tau_{21}^{J_2}\}$, with shaded bands denoting 1σ variations across the ensembles of trained models. The dashed gray line shows the performance of the full phase space method from Ref. [17], whereas the dashed green line shows that of the pre-trained foundation model OmniLearn from Ref. [21].

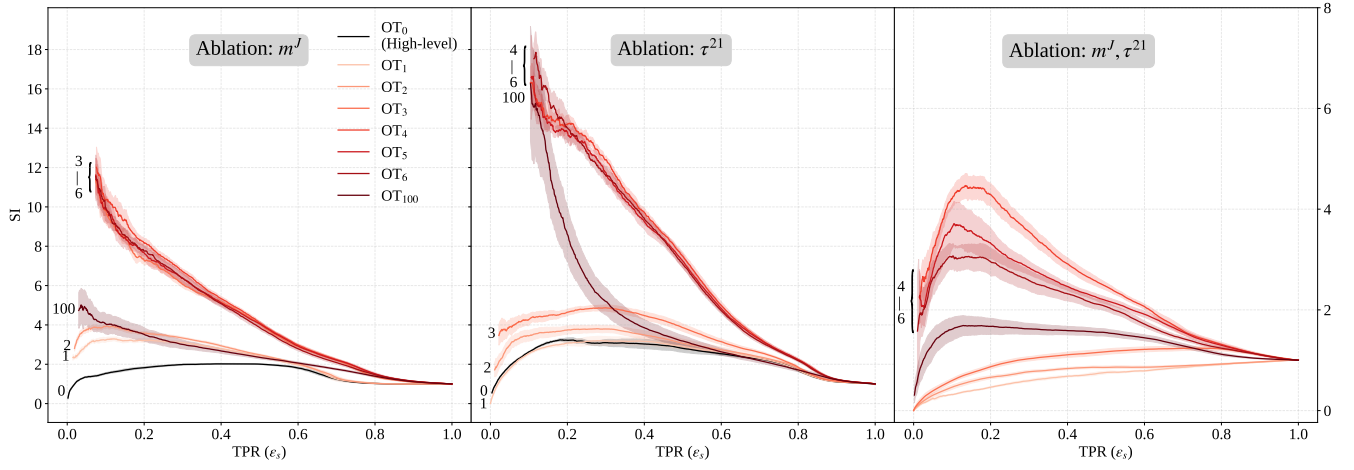


FIG. 5: The SI curves for the R&D1 dataset using BDT ensembles as the classifier at $S/B = 0.63\%$. *Left:* The input features are $\{\tau_{21}^{J_1}, \tau_{21}^{J_2}\}$ and different number of PCA modes for the OT representation (the group of red lines). *Middle:* The input features are $\{m_{J_1}, m_{J_2}\}$ and different number of PCA modes for the OT representation. Note that the middle subplot shares the same y -axis with the leftmost subplot. *Right:* The input features only include different number of PCA modes for the OT representation. Note that the rightmost subplot has its own y -axis to the right. Shaded bands denote 1σ variations across the ensembles of trained models.